

The Global 21 cm Absorption from Cosmic Dawn with Inhomogeneous Gas Distribution

Yidong Xu¹, Bin Yue¹, Xuelei Chen^{1,2,3}

ABSTRACT

We make an analytical estimate of the maximum 21 cm absorption signal from the cosmic dawn, taking into account the inhomogeneity of gas distribution in the intergalactic medium (IGM) due to non-linear structure formation. The gas located near halos is over-dense but adiabatically heated, while the gas far from halos is under-dense and hence cooler. The cumulative effect of adiabatic heating and cooling from this gas inhomogeneity results in a reduction in the maximum global 21 cm absorption depth by about 40% as compared with homogeneous IGM model, assuming saturated coupling between the spin temperature of neutral hydrogen (HI) and the adiabatic gas kinetic temperature.

Subject headings: Cosmology: theory — dark ages, reionization, first stars — intergalactic medium

1. Introduction

The EDGES experiment (Experiment to Detect the Global Epoch of reionization Signature; Bowman & Rogers 2010) has recently announced the discovery of an absorption feature in the global spectrum of the sky around 78 MHz (Bowman et al. 2018). If this is due to the global 21 cm absorption signal from the cosmic dawn (Madau et al. 1997; Chen & Miralda-Escudé 2004, 2008; Furlanetto 2006), it amounts to 21 cm brightness temperature $\delta T_{21} = -500_{-500}^{+200}$ mK (99% confidence level, Bowman et al. 2018), which is much deeper than what is typically expected from standard models of the diffuse intergalactic medium (IGM), indeed even deeper than the largest possible absorption by the adiabatically cooled primordial gas. To explain this excess absorption, various models are developed, e.g. to cool the gas by interaction with cold dark matter (e.g. Barkana 2018; Muñoz & Loeb 2018; Fialkov et al. 2018;

Barkana et al. 2018; Slatyer & Wu 2018; Hirano & Bromm 2018; Muñoz et al. 2018), or to increase the background radiation intensity (e.g. Feng & Holder 2018; Ewall-Wice et al. 2018; Fraser et al. 2018).

Previous calculation of the expected global signal level considered only the diffuse IGM with the mean cosmic density, or with the large-scale density field from relatively low-resolution simulations (e.g. Cohen et al. 2017). However, the matter density surrounding halos is enhanced (Barkana 2004; Prada et al. 2006; Betancort-Rijo et al. 2006), which could make a significant contribution to the total absorption signature. On the other hand, as the virial temperatures of halos at the redshifts of interest are typically higher than the CMB temperature, the neutral gas inside halos could produce weak 21 cm emission signals which compensate part of the absorption signal (Yue et al. 2009). Here we re-evaluate the total 21cm global signal by focusing on the cold gas surrounding the halos which is neither virialized nor heated by astrophysical or exotic radiations.

While the absorption depth is proportional to the gas density, adiabatic heating would increase the temperature and leads to only a small increase in the absorption from over-dense regions in the IGM (Barkana 2018). The gas in the voids on the

¹Key Laboratory for Computational Astrophysics, National Astronomical Observatories, Chinese Academy of Sciences, Beijing 100101, China

²School of Astronomy and Space Science, University of Chinese Academy of Sciences, Beijing 100049, China

³Center for High Energy Physics, Peking University, Beijing 100871, China

other hand, would produce a less weak absorption due to the opposite effects. The overall effect of the inhomogeneous gas distribution is not yet quantified. Using a high redshift point source as the background, Xu et al. (2011) computed the 21 cm absorption signals from individual minihalos and dwarf galaxies, including both the gas contents inside and around the halos. With similar algorithm for computing the optical depth, but using the CMB as the background radio source, we can derive the global 21 cm signal from the cumulative absorption from the inhomogeneous gas distribution within and around halos arising from non-linear structure formation. We find that before the occurrence of significant X-ray heating in the early Universe, the maximum global 21 cm absorption depth is reduced when compared with the case of homogeneous IGM, thanks to the adiabatic heating effect of the over-dense gas surrounding the halos.

Throughout this paper, we assume the Λ CDM model and adopt the Planck 2015 cosmological parameters (Planck Collaboration et al. 2016): $\Omega_b = 0.0485$, $\Omega_c = 0.259$, $\Omega_\Lambda = 0.692$, $H_0 = 67.81 \text{ km s}^{-1} \text{ Mpc}^{-1}$, $\sigma_8 = 0.8149$ and $n_s = 0.9677$. However, the effect discussed here are not sensitive to the parameter values.

2. The 21 cm absorption line from the gas around one halo

We begin by calculating the 21 cm absorption line profile from the neutral hydrogen surrounding an *isolated* halo. Note that we also include the absorption from the gas inside halos assuming collisional ionization equilibrium (Xu et al. 2011), but this part of gas only has a small contribution to the total absorption. As we shall find from the calculations below, the main contribution to the optical depth is from the gas outside of halos with the adiabatic temperature much lower than the virial temperature. The 21 cm optical depth of an isolated object can be derived from the integral of the absorption coefficient along the line of sight

(Furlanetto & Loeb 2002; Xu et al. 2011):

$$\tau(\nu) = \frac{3 h_P c^3 A_{10}}{32 \pi^{3/2} k_B} \frac{1}{\nu_{10}^2} \times \int_{-\infty}^{+\infty} dx \frac{n_{\text{HI}}(r)}{b(r) T_S(r)} \exp \left[- \frac{(u(\nu) - \bar{v}(r))^2}{b^2(r)} \right], \quad (1)$$

where h_P is the Planck constant, c is the speed of light, $A_{10} = 2.85 \times 10^{-15} \text{ s}^{-1}$ is the Einstein coefficient for the spontaneous decay of the 21 cm transition, and k_B is the Boltzmann constant. In the integrand, n_{HI} , T_S , and b are the neutral hydrogen number density, the spin temperature, and the Doppler parameter of the gas, respectively. $b(r) = \sqrt{2 k_B T_K(r) / m_H}$, $u(\nu) \equiv c(\nu - \nu_{10}) / \nu_{10}$ with $\nu_{10} = 1420.4 \text{ MHz}$ being the rest frame frequency of the 21 cm transition, and $\bar{v}(r)$ is bulk velocity of gas projected to the line of sight at the radius r . The coordinate x is related to the radius r by $r^2 = (\alpha r_{\text{vir}})^2 + x^2$, where α is the impact parameter of the penetrating line of sight in units of the halo virial radius r_{vir} .

The cold over-dense gas around the halos could absorb the CMB photons and enhance the 21 cm absorption with respect to that due to only the diffuse IGM. However, even in the absence of X-ray heating from the first astrophysical sources, the over-dense gas surrounding halos is adiabatically heated according to $T_K \propto \rho^{2/3}$, and due to dearth of metals, the cooling is very slow. This counteracts and reduces the density enhancement effect. To estimate the maximum level of absorption, here we assume saturated coupling between the spin temperature and the gas kinetic temperature by the Ly α radiation via the Wouthuysen-Field effect (Wouthuysen 1952; Field 1958; Hirata 2006), i.e. $T_S = T_K$.

In addition to the enhanced density, the gravitational potential of a halo also induces infall of the surrounding gas (Barkana 2004; Prada et al. 2006; Betancort-Rijo et al. 2006), and the gas outside the virial radius has a velocity which is determined by the competition between the infall and the Hubble flow. The gas density and infall velocity profiles are calculated with the spherical collapse ‘‘Infall Model’’ (Barkana 2004)¹.

¹The ‘‘Infall Model’’ code is publicly available at <http://wise-obs.tau.ac.il/~barkana/codes.html>.

The optical depth profiles of a halo with mass $10^8 M_\odot$ at redshift $z = 17$ are plotted in Fig. 1 for a few impact parameter values. The peak optical depth is significantly enhanced for lines of sight penetrating through the gas just outside the virial radius (the dotted, dot-dashed, and long-dashed lines for $\alpha = 1, 3,$ and $10,$ respectively), as compared to the optical depth caused by the IGM of the mean density (the short-dashed line for $\alpha = 30$).

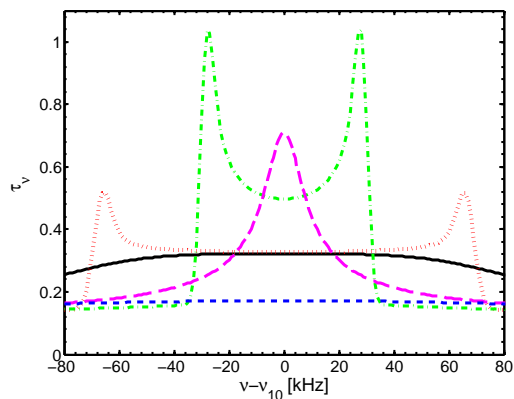


Fig. 1.— The optical depth profiles for a few line of sights passing through the gas around an isolated halo with mass $M = 10^8 M_\odot$ at $z = 17$, assuming adiabatic gas temperature. The impact parameters of the different curves are $\alpha = 0$ (solid black), 1 (dotted red), 3 (dot-dashed green), 10 (long-dashed magenta), and $\alpha = 30$ (short-dashed blue), respectively.

The line profiles in Fig.1 can be understood by noting the different contributions from the gas located at different radii (Xu et al. 2011). Let $\nu_p(r)$ be the peak frequency of optical depth generated

by gas located at radius r , the absorption is shifted from the line center by

$$\nu_p(r) - \nu_{10} = \frac{\bar{v}(r)}{c} \nu_{10}. \quad (2)$$

Because of the infall, the absorption line is significantly broadened, dramatically exceeding the thermal broadening. The segmental contributions to the optical depth from the gas located at different radii are plotted in Fig.2. The gas located just outside the r_{vir} has the largest infall velocity, and the corresponding absorption lies at the largest distance to the line center in the upper panel. Its optical depth is however a bit suppressed because of the higher temperature of the denser gas. As the radius increases, the τ_ν profile gets closer to the line center because of the decreasing infall velocity. At the turn-around point, where the gas velocity changes from infall-dominated to Hubble-flow-dominated, the two absorption lines created by the two segments on both sides of the halo converge into one at the line center, and they contribute substantially to the central optical depth. After that, the τ_ν profiles that come from larger radii leave the line center again, and when it goes out of the region influenced by the halo’s gravity, and the density drops to the cosmic mean value, we recover the IGM mean optical depth.

Therefore, for a line of sight penetrating through an isolated halo at cosmic dawn with a small impact parameter, the optical depth is significantly enhanced, not only because of the enhanced density, but also because of the infalling velocity which re-distributed the absorption depth. In order to correctly determine the optical depth and the profile of the 21 absorption lines from individual halo surroundings, it is important to take into account both the effect of enhanced density and the infalling velocity of the gas. However, when considering the overall absorption by the gas surrounding all halos, the infalling velocity which acts as a re-distributor, may not have such a significant effect. The adiabatic heating/cooling of the over-dense/under-dense gas, on the other hand, may have a cumulative effect. Note that here we have assumed that the gas follows the dark matter distribution according to the infall model, and the gas fraction equals to the cosmic mean baryonic fraction everywhere. In the following, we will investigate the relative effects of

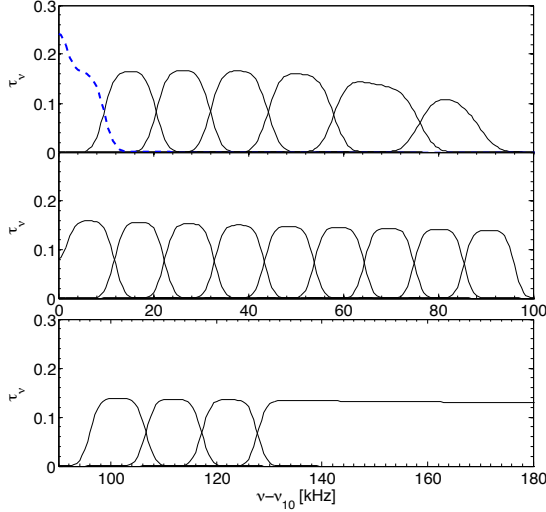


Fig. 2.— Contributions to the optical depth from the gas at different radii, for a line of sight penetrating through the center of an isolated halo of mass $10^8 M_\odot$ at redshift 17. *Upper panel:* the solid lines from right to left correspond to the absorptions by segments of $(1-2) r_{\text{vir}}$, $(2-3) r_{\text{vir}}$, $(3-4) r_{\text{vir}}$, $(4-5) r_{\text{vir}}$, $(5-6) r_{\text{vir}}$ and $(6-7) r_{\text{vir}}$, respectively, and the dashed line represents the absorption by the segment of $(7-8) r_{\text{vir}}$. *Central panel:* the 9 solid lines from left to right correspond to the absorptions by segments of $1 r_{\text{vir}}$ each starting from $8 r_{\text{vir}}$. *Bottom panel:* the 3 solid lines from left to right correspond to the absorptions by segments of $1 r_{\text{vir}}$ each starting from $17 r_{\text{vir}}$, and the last curve represents the integral absorption from 20 to $100 r_{\text{vir}}$.

enhanced density, the infalling velocity, as well as the adiabatic heating/cooling, on the cumulative absorption from the gas around non-isolated halos, with the total gas content normalized.

3. The 21 cm spectrum from cumulative gas around all halos

The radiative transfer equation in the Rayleigh-Jeans limit gives the emergent 21 cm brightness temperature:

$$T_b = T_{\text{CMB}}^{\text{out}} + T_{\text{em}}^{\text{out}} = T_{\text{CMB}} e^{-\tau_{\text{tot}}} + \int_0^{\tau_{\text{tot}}} T_S(\tau) e^{-\tau} d\tau, \quad (3)$$

where $T_{\text{CMB}}^{\text{out}}$ is the contribution from the background radiation, and $T_{\text{em}}^{\text{out}}$ is the contribution from the gas emission. Here T_{CMB} is the CMB temperature at redshift z , and τ_{tot} is the integrated optical depth from all gas in the Universe that could contribute to the 21cm absorption at the corresponding frequency. We have to account for the gas surrounding all halos, from the regions with enhanced density near the halos to the regions with lower density faraway. Accordingly, the gas is adiabatically heated or cooled depending on the local density. In the case of homogeneous spin temperature of HI, Eq.(3) reduces to

$$T_b = T_{\text{CMB}} e^{-\tau_{\text{tot}}} + T_S (1 - e^{-\tau_{\text{tot}}}). \quad (4)$$

However, here we have to use the original form of Eq.(3) in order to account for the inhomogeneity in the gas temperature.

In the above we find that the infall velocity is important for broadening the absorption line produced by each halo. As a consequence, the gas with the bulk velocity of $\bar{v}(r)$ can contribute to the absorption at the central 21 cm frequency at z , which is at a comoving distance $\Delta l = (1+z)\bar{v}(r)/H(r)$ away from it, so for the 21cm optical depth corresponding to a certain redshift z , one needs to integrate the contribution up to distance Δl_{max} away, which is determined by the maximum infall velocity which depends on the halo mass. The integrated optical depth of the 21 cm absorption at an intrinsic frequency ν_{10} at redshift z_c is then

$$\begin{aligned} \tau_{\text{tot}}(z_c) = & \frac{3 h_P c^3 A_{10}}{32 \pi^{3/2} k_B} \frac{1}{\nu_{10}^2} \\ & \times \int_{-\infty}^{+\infty} dl(z) \int_{M_{\text{min}}}^{M_{\text{max}}} \frac{dn}{dM}(M, z) dM \\ & \times \int_0^{\alpha_{\text{max}}} 2 \pi r_{\text{vir}}^2(M, z) (1+z)^2 \alpha d\alpha \\ & \times \int_{-x_{\text{max}}}^{+x_{\text{max}}} dx \frac{n_{\text{HI}}(r)}{b(r) T_S(r)} \exp \left[- \frac{(u(\nu) - \bar{v}(r))^2}{b^2(r)} \right]. \end{aligned} \quad (5)$$

Here ν is related to ν_{10} by $\nu/(1+z) = \nu_{10}/(1+z_c)$, $x_{\text{max}} = r_{\text{vir}} \sqrt{\alpha_{\text{max}}^2 - \alpha^2}$, and dn/dM is the halo mass function, for which we adopt the Sheth-Tormen form (Sheth & Tormen 2002). We integrate the absorption by the gas content out to a maximum impact parameter α_{max} , which is set

to be half of the mean halo distance determined by the minimum halo mass under consideration; the gas located at farther than this distance would probably be influenced by the gravitational potential of a neighboring halo, and this part of gas is taken into account as contribution from the neighboring halo surrounding.

For a patch of HI gas from one halo, the emission term in the emergent brightness can be written as

$$\begin{aligned}
T_{\text{em},1\text{h}}^{\text{out}} &= \int_{-x_{\text{max}}}^{+x_{\text{max}}} T_{\text{S}}(x) e^{-\tau(x)} \kappa_{\nu}(x) dx \\
&= \frac{3 h_{\text{P}} c^3 A_{10}}{32 \pi^{3/2} k_{\text{B}}} \frac{1}{\nu_{10}^2} \\
&\times \int_{-x_{\text{max}}}^{+x_{\text{max}}} e^{-\tau(x)} \frac{n_{\text{HI}}(r)}{b(r)} \exp \left[-\frac{(u(\nu) - \bar{v}(r))^2}{b^2(r)} \right] dx,
\end{aligned} \tag{6}$$

where

$$\begin{aligned}
\tau(x) &= \frac{3 h_{\text{P}} c^3 A_{10}}{32 \pi^{3/2} k_{\text{B}}} \frac{1}{\nu_{10}^2} \\
&\times \int_{-x_{\text{max}}}^x \frac{n_{\text{HI}}(r')}{b(r') T_{\text{S}}(r')} \exp \left[-\frac{(u(\nu) - \bar{v}(r'))^2}{b^2(r')} \right] dx'.
\end{aligned} \tag{7}$$

Adding up the emission from all halos, the total emission term in Eq.(3) is then

$$\begin{aligned}
T_{\text{em}}^{\text{out}} &= \frac{3 h_{\text{P}} c^3 A_{10}}{32 \pi^{3/2} k_{\text{B}}} \frac{1}{\nu_{10}^2} \\
&\times \int_{-\infty}^{+\infty} dl(z) \int_{M_{\text{min}}}^{M_{\text{max}}} \frac{dn}{dM}(M, z) dM \\
&\times \int_0^{\alpha_{\text{max}}} 2 \pi r_{\text{vir}}^2(M, z) (1+z)^2 \alpha d\alpha \\
&\times \int_{-x_{\text{max}}}^{+x_{\text{max}}} e^{-\tau(x)} \frac{n_{\text{HI}}(r)}{b(r)} \exp \left[-\frac{(u(\nu) - \bar{v}(r))^2}{b^2(r)} \right] dx.
\end{aligned} \tag{8}$$

The observed 21 cm signal is the differential brightness temperature relative to the CMB, i.e.

$$\delta T_{21}(z_c) = \frac{T_{\text{b}}(z_c) - T_{\text{CMB}}(z_c)}{1 + z_c}. \tag{9}$$

The 21 cm signal depends on the neutral gas content of matter in and around halos. Small halos have shallow gravitational potential and could hardly retain enhanced gas density around them,

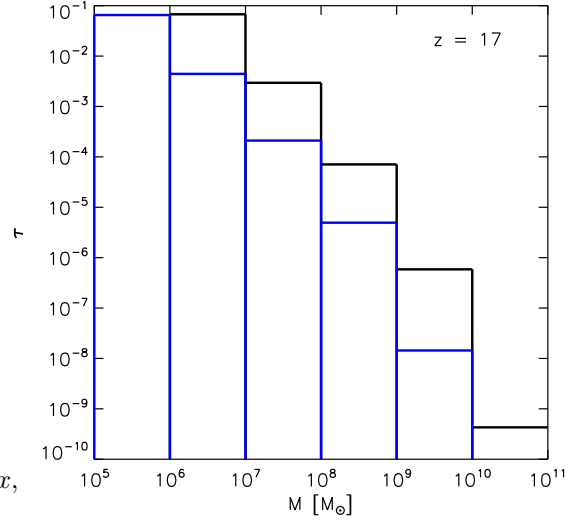


Fig. 3.— The optical depth contributed from the gas surrounding halos of different mass ranges at redshift 17. The blue histogram shows the contribution of various halos assuming $M_{\text{min}} = 10^5 M_{\odot}$, and the black histogram shows the result with $M_{\text{min}} = 10^6 M_{\odot}$.

while very massive halos would have high probability of hosting the first stars or galaxies at cosmic dawn and get the surrounding gas ionized. Beyond redshift 7, for an early X-ray background less than 20% of the intensity today, the characteristic mass M_{C} at which halos on average could retain half of their baryons is $\sim 10^6 M_{\odot}$ (Xu et al. 2011). Halos with lower mass could also have gas content in and around them, but we take this mass limit as the minimum mass for a halo that could induce *enhanced* gas density *outside* of it. The gas around lower mass halos is taken into account by the integration up to the maximum impact parameter, well into the IGM. In the following, we consider halos with masses in the range of $[10^6 M_{\odot} - 10^{11} M_{\odot}]$ which cover the characteristic halo mass and most of the halos that could retain cold and neutral gas around them. We will also show results with $M_{\text{min}} = 10^5 M_{\odot}$, in order to investigate the effect of this uncertain mass limit. The higher mass halos have dense infalling gas around them, and even the adiabatic heating could raise the gas temperature in the nearest region above

the CMB temperature at the time. This effect, in combination with the much lower number density of massive halos, results in negligible contribution from the gas surrounding halos more massive than $10^{10}M_{\odot}$ (as seen from Fig. 3), and we conservatively set the upper limit to be $10^{11}M_{\odot}$. We also tried including the contribution from the gas in and around halos up to $10^{12}M_{\odot}$ assuming no ionization, and found that it made a negligible correction to the total optical depth.

Using the mean density profile predicted by the “infall model”, the different contributions to the optical depth from the gas surrounding halos of different mass ranges are plotted with the histogram in Fig. 3. We find that the gas surrounding low mass halos dominates the absorption. Combining the background radiation attenuated by the total optical depth $T_{\text{CMB}}^{\text{out}}$, and the gas emission term $T_{\text{em}}^{\text{out}}$, the thick solid line in Fig. 4 shows the maximum 21 cm absorption signal, or the minimum 21 cm brightness temperature evolution during the cosmic dawn, when the inhomogeneous gas distribution with inhomogeneous temperature is taken into account. The previous prediction in which all gas is homogeneously distributed in the IGM, is plotted with the thick dashed line. We find that the maximum 21 cm global spectrum signal expected in the standard model is reduced by a factor of about 40% as compared with previous prediction with homogeneous IGM, due to the inhomogeneity in the gas distribution.

Note that there is large uncertainty in the density profile around halos, even in the ideal case predicted by the infall model (see the large scatter in Fig. 3 of Barkana 2004). In the above calculation, we have neglected the halo clustering, and the infall model predicts the density profile within a biased region with an initial over-density. In a more realistic situation, the halos tend to cluster in over-dense regions, and the distances between halos in these regions are smaller than the mean halo distance estimated from the mean halo number density. If we integrate the gas content up to half of the mean halo distance around each halo, we would over-count the total gas amount. Here we introduce a normalization factor to the mean density profile predicted by the model, i.e. $\rho(r) = C[1 + \delta(r)]\bar{\rho}$, where the normalization factor C is determined by requiring the conservation of the total gas content in the Universe. We

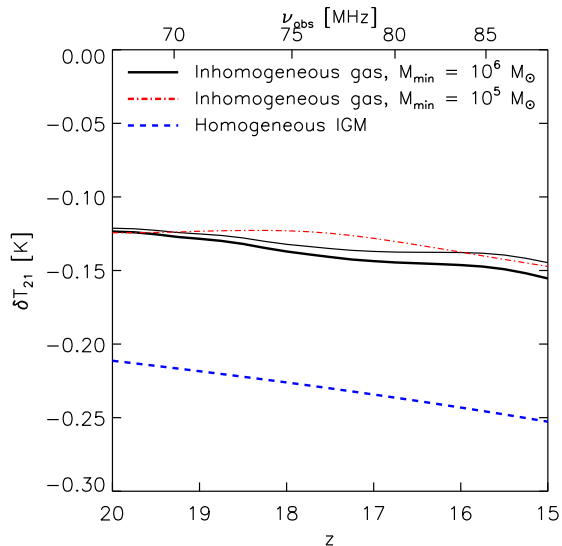


Fig. 4.— The 21 cm global spectrum from the adiabatic gas before reionization assuming saturated Ly α coupling between the HI spin temperature and the gas kinetic temperature. The thick solid line shows the maximum signal from the inhomogeneous gas due to non-linear structure formation in the default model with $M_{\text{min}} = 10^6 M_{\odot}$, the thin solid line shows the signal with normalized gas content, and the dot-dashed line shows the signal with normalized gas content assuming $M_{\text{min}} = 10^5 M_{\odot}$. For comparison, the maximum signal from the homogeneous IGM is plotted with dashed line.

find that for the mean density profile predicted by the “Infall Model”, this normalization factor ranges from ~ 0.87 ($z = 20$) to ~ 0.67 ($z = 15$) if the M_{min} that can induce enhanced surrounding density is $10^6 M_{\odot}$, or from ~ 0.69 ($z = 20$) to ~ 0.58 ($z = 15$) if $M_{\text{min}} = 10^5 M_{\odot}$. It is smaller than 1 as expected. The results with normalized gas content are shown in Fig. 4 with thin solid line for $M_{\text{min}} = 10^6 M_{\odot}$ and thin dot-dashed line for $M_{\text{min}} = 10^5 M_{\odot}$, respectively. The signal is further reduced due to the normalized gas content, but the decrement is fairly small because of the roughly $\rho^{1/3}$ scaling of the optical depth in the adiabatic case. Note that the detailed gas density profile depends on the halo formation history and should vary from place to place depending on the

local gravitational potential.

We also investigate the maximum signal from inhomogeneous gas density but with homogeneous temperature without adiabatic heating or cooling effect. We find that the inhomogeneous distribution of the gas density alone weakly decreases the global 21 cm absorption (by $\sim 3\%$ for $M_{\min} = 10^6 M_{\odot}$ and by $\sim 7\%$ for $M_{\min} = 10^5 M_{\odot}$ at redshift 17), whereas in combination with the adiabatic heating effect reduces the absorption signal by $\sim 40\%$.

The uncertainty in the minimum halo mass that could induce a higher density in the surrounding gas does affect the contribution of the absorption from different halo surroundings as seen in Fig. 3. However, by integrating the contribution from all the HI gas in the Universe, the overall effect of the adiabatic heating/cooling due to the inhomogeneity is not very sensitive to the assumed M_{\min} , and the results assuming $M_{\min} = 10^6 M_{\odot}$ and that with $M_{\min} = 10^5 M_{\odot}$ differ by less than 10%. We also test the effect of the infall velocity, and find that by integrating over the gas surrounding all halos, the infall velocity induced by individual halos shifts the contribution of the absorption from different halos, but only has a negligible effect on the overall absorption depth.

4. Conclusions and discussions

In this work, we have re-calculated the maximum signal of the global 21 cm spectrum from the cosmic dawn taking into account of the inhomogeneous distribution of gas in the IGM due to non-linear structure formation. Assuming adiabatic gas temperature and saturated Ly α coupling between the HI spin temperature and the gas kinetic temperature, and using the density profile of halo surroundings predicted by the infall model (Barkana 2004), we integrate the absorption from the gas surrounding almost all halos that could retain over-dense neutral and cold gas nearby. We find that the maximum global 21 cm signal that could possibly be reached in the standard model is even weaker than previously thought, by a factor of $\sim 40\%$, mainly because of the adiabatic heating of the inhomogeneous gas around non-linear structures. This result further escalates the tension between the standard model prediction and the observational evidence of the deep absorption

signal (Bowman et al. 2018).

One caveat in the above analytical estimation is that the infall model we adopted was developed for isolated halos. In fact, neighboring halos could modify the density distribution and the velocity profile around the halos due to the tidal effect that is inevitable in the realistic environments, and hence affect the predicted optical depth. In addition, halo clustering, for which we have not accounted, could further reduce the accuracy of the model prediction. The gas fractions around halos of different masses are also quite uncertain, depending on the local gravitational potential and the photon-evaporation effect once the first stars formed. More accurate gas distribution in the Universe requires high-resolution hydrodynamic simulation. Therefore, the result presented here should only be taken as qualitative. However, the reduced 21 cm absorption is caused by the inhomogeneous distribution of the gas and the related adiabatic heating effect, which is inevitable no matter what density profile we adopt. A more precise estimation of the evolution of the global 21 cm signal also requires detailed modeling of the first star formation and the evolution in the Ly α background. We plan to implement more realistic calculation of the early Ly α background level and the HI spin temperature in a future work.

Recently, Venumadhav et al. (2018) have found that in the absence of the first ionizing sources, there is extra heating by the CMB, which may induce a $\sim 10\%$ correction on the gas temperature, and will further reduce the signal. We have not included this effect in this work, but combining these two effects, we conclude that the maximum global 21 cm signal from the cosmic dawn should be weaker than the previous estimate.

Any X-ray heating in the early Universe would be an additional effect to further decrease the absorption level. Depending on the nature of the X-ray sources (stellar sources, X-ray binaries, QSOs, or other exotic sources), the evolutionary behavior of its effect on the global 21 cm signal would be different from the adiabatic heating effect that is expected to be smoother in redshift. Also, the angular dependence of the 21 cm fluctuations may be used to distinguish the X-ray heating effect from the adiabatic heating effect. The adiabatic heating effect is correlated with the spatial distribution of predominantly small halos, while the temperature

fluctuations from X-ray heating would dominate the 21 cm fluctuations on larger scales depending on the X-ray sources (Ross et al. 2018).

This work is supported by the Chinese Academy of Sciences (CAS) Strategic Priority Research Program XDA15020200, the CAS Frontier Science Key Project QYZDJ-SSW-SLH017, the National Natural Science Foundation of China (NSFC) key project grant 11633004, the NSFC-ISF joint research program No. 11761141012, and the MoST 2016YFE0100300. BY acknowledges the support of the Hundred Talents (Young Talents) program from the CAS, the NSFC grant 11653003 and the NSFC-CAS joint fund for space scientific satellites No. U1738125.

REFERENCES

- Barkana, R. 2004, *MNRAS*, 347, 59
- . 2018, *Nature*, 555, 71
- Barkana, R., Outmezguine, N. J., Redigolo, D., & Volansky, T. 2018, *ArXiv e-prints*, 1803.03091
- Betancort-Rijo, J. E., Sanchez-Conde, M. A., Prada, F., & Patiri, S. G. 2006, *ApJ*, 649, 579
- Bowman, J. D., & Rogers, A. E. E. 2010, *Nature*, 468, 796
- Bowman, J. D., Rogers, A. E. E., Monsalve, R. A., Mozdzen, T. J., & Mahesh, N. 2018, *Nature*, 555, 67
- Chen, X., & Miralda-Escudé, J. 2004, *ApJ*, 602, 1
- . 2008, *ApJ*, 684, 18
- Cohen, A., Fialkov, A., Barkana, R., & Lotem, M. 2017, *MNRAS*, 472, 1915
- Ewall-Wice, A., Chang, T.-C., Lazio, J., Doré, O., Seiffert, M., & Monsalve, R. A. 2018, *ArXiv e-prints*, 1803.01815
- Feng, C., & Holder, G. 2018, *ArXiv e-prints*, 1802.07432
- Fialkov, A., Barkana, R., & Cohen, A. 2018, *ArXiv e-prints*, 1802.10577
- Field, G. B. 1958, *Proceedings of the IRE*, 46, 240
- Fraser, S. et al. 2018, *ArXiv e-prints*, 1803.03245
- Furlanetto, S. R. 2006, *MNRAS*, 371, 867
- Furlanetto, S. R., & Loeb, A. 2002, *ApJ*, 579, 1
- Hirano, S., & Bromm, V. 2018, *ArXiv e-prints*, 1803.10671
- Hirata, C. M. 2006, *MNRAS*, 367, 259
- Madau, P., Meiksin, A., & Rees, M. J. 1997, *ApJ*, 475, 429
- Muñoz, J. B., Dvorkin, C., & Loeb, A. 2018, *ArXiv e-prints*, 1804.01092
- Muñoz, J. B., & Loeb, A. 2018, *ArXiv e-prints*, 1802.10094
- Planck Collaboration et al. 2016, *A&A*, 594, A13
- Prada, F., Klypin, A. A., Simonneau, E., Betancort-Rijo, J., Patiri, S., Gottlöber, S., & Sanchez-Conde, M. A. 2006, *ApJ*, 645, 1001
- Ross, H. E., Dixon, K. L., Ghara, R., Iliev, I. T., & Mellema, G. 2018, *ArXiv e-prints*, 1808.03287
- Sheth, R. K., & Tormen, G. 2002, *MNRAS*, 329, 61
- Slatyer, T. R., & Wu, C.-L. 2018, *ArXiv e-prints*, 1803.09734
- Venumadhav, T., Dai, L., Kaurov, A., & Zaldarriaga, M. 2018, *ArXiv e-prints*, 1804.02406
- Wouthuysen, S. A. 1952, *AJ*, 57, 31
- Xu, Y., Ferrara, A., & Chen, X. 2011, *MNRAS*, 410, 2025
- Yue, B., Ciardi, B., Scannapieco, E., & Chen, X. 2009, *MNRAS*, 398, 2122